Proceedings of the XVIII International Symposium on Dynamic Problems of Mechanics (DINAME 2019),
M.A. Savi, T.G. Ritto and W.M. Bessa (editors), ABCM, Buzios, RJ, Brazil, March 10th to 15th, 2019

Closed-loop multiobjective optimization of piezoelectric patches for active vibration control of a rectangular plate

Augusto Hirao Shigueoka[1], **Hélio Jacinto Cruz Neto**[1] , **Filipe Moraes Horiy**[1] **and Marcelo Areias Trindade**[1]

[1] Department of Mechanical Engineering, São Carlos School of Engineering, University of São Paulo, Av. Trabalhador São-Carlense, 400, 13566-590, São Carlos – SP, Brazil

Abstract: The combination of modal filters with Direct Velocity Feedback (DVF) is a popular choice of active vibration control of flexible structures due to its simplicity. Even though some recent works have improved the design of spatial modal filters, even including sensor positioning, most of them focused on the attenuation of the spillover by only predefining the modes to be filtered in and considering any other mode as undesired spillover. In this work a closed-loop optimization is performed using a multiobjective Genetic Algorithm (GA). One of the objectives is the attenuation of select modes of vibration in the structure, while the other is the frequency bandwidth over which the system guarantees stability. The Pareto Front is found and the results for both rectangular and optimal placement shows the compromise between the two objectives. Then the optimal designs for three different frequencies are compared. We conclude that i) our closed-loop optimization also attenuates modes which were not required to be damped ii) sensor placement is not very advantageous over fixed sensors when the frequency bandwith used in the design is too narrow or too short.

Keywords: Vibration control, piezoelectric materials, sensor networks, spatial modal filters, optimization

INTRODUCTION

Piezoelectric ceramics in the form of patches are highly suited for sensing and actuation when dealing with vibration suppression on flexible structures, due to their low weight and simple construction Leo (2007). A strategy of active vibration control called Independent Modal Space Control (IMSC) was widely studied by the scientific community during 1980-2000. By designing the control system in the space generated by the modal shapes of the structure, it was possible to alter the dampening of each mode individually, one of the conditions being that the number of sensors be equal to the number of modes of vibration present in the model Meirovitch and Öz (1980), Meirovitch and Baruh (1982).

The knowledge that sensor and actuator placement affects the performance of a vibration control system is not recent Meirovitch (1990), but the first studies on optimal placement of piezoelectric transducers only started around the 2000s Han and Lee (1999). Then it was shown in Pagani, Jr and Trindade (2009) that it is possible to work with less sensors than the number of modes present in the model as long as a sensor placement optimization is performed. It was also shown how the increase in the number of modes in the model degrades the performance of the spatial sensor, with observability and controllability spillover limiting its use for stability in vibration control.

Despite optimal sensor placement not being a completely recent field of research, the computing power now available lets researchers numerically optimize systems which were priorly limited to analytical cases with quite limiting hypothesis, such as regular geometry, existence of closed-form solutions, sensors whose effects in the model response may be neglected etc. A search using the keywords “sensor placement” will reveal several recent works. In the subfield of vibration control, there is Cinquemani, Ferrari and Bayati (2015), who showed that spillover effects are equivalent to off-diagonal coefficients in the damping matrix of the closed-loop system, when using Direct Velocity Feedback (DVF) with Meirovitch’s (IMSC).

Still, most works available in the literature still optimize an open-loop system. For example, Preumont et al. (2003) defines a target function to be approximated as closely as possible from the available outputs. The downside of such method is that the control designer has to choose a priori which modes should be filtered in, while all the others are to be affected as little as possible. It should be noted, though, that not every kind of spillover is necessarily detrimental, that is, it is possible to have some kind of spillover which increases the structure’s damping. As long as it does not incur an excessive increase in control effort, then it will be actually beneficial. In the closed-loop optimization, which is performed in this work, such predefinition of which modes should be sensed or actuated on is not made. Even in recent works, such as Cinquemani, Ferrari and Bayati (2015), Gonçalves, de Leon and Perondi (2017), Khushnood, Xiaogang and Naigang (2018) and Xue, Igarashi and Kachi (2018), which use different metrics for sensor positioning, the target modes are predefined and only after that the optimization process is carried on. Most studies use a metric based on either the observability or controlability Grammians, or both. Some even include the spillover effect. The review Gupta, Sharma and Takur (2010) lists other criteria for optimization of sensor placement. However, being able to observe or control only the modes of interest may be too restrictive. In a previous study Horiy, Shigueoka and Trindade (2017), the best modal sensor configuration attenuated a mode that was not required to be damped. The optimization was able to find a

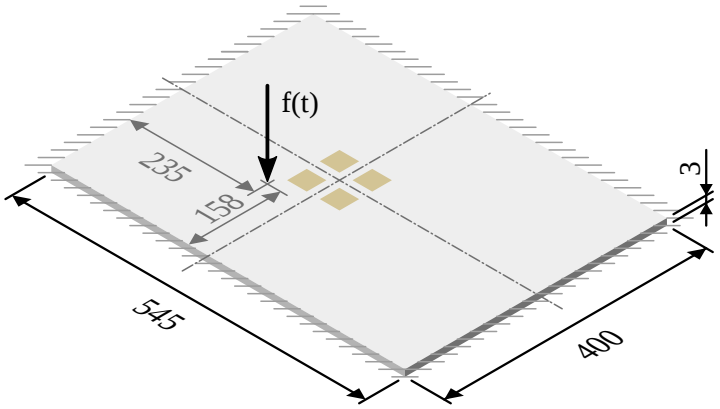

Figure 1: Schematic representation of the system being studied. Dimensions are given in millimetres.

weighting which leveled the control effort, so that there was a better exploitation of the actuator along the bandwidth and even included some mode sensing which would be counted as spillover in the traditional approach. However, the GA was computationally expensive as an control system optimizer. This works compares the optimal found from GA and an alternative, less computationally expensive method, the Incomplete State Feedback (Cruz Neto and Trindade, 2017), whose formulation is described in Cruz Neto (2018).

Another commonly used the hypothesis is that the piezoelectric transducers do not substantially affect the response of the structure, for example Hsu, Lin and Gaul (1998); Sadri, Wright and Wynne (1999); Biglar et al. (2015). Such hypothesis may be valid depending on the construction of the transducers and the coverage of the analysed structure. The more piezoeletric patches start to cover it, though, the more they start to affect the structure's response. On the bright side, neglecting the effects of the transducer does help in reducing the computational cost of the analysis, since it is not necessary to create a new model for each transducer placement. When adopting such simplification, a posterior validation is recomended, as done in Pagani, Jr and Trindade (2009).

In short, the previous works have always made use of at least one of the following simplifying assumptions:

- an optimal modal filter for mode isolation is optimal for modal control;
- the effects of the transducers on the model response are negligible;
- the optimal control system can be found from observability, controllability and spillover considerations alone.

This work does not assume any of the above hypothesis. When performing the optimization, a finite element model is generated for each sensor placement and the closed-loop system is explicitly computed in order to access its performance. This approach has the drawback of being too costly in terms of computational power. On the other hand, the solution found in this brute-force method showed which shortcomings the other approaches have in finding the optimal design for the control system.

METHODOLOGY

In order to investigate the effect of sensor positioning on a flexible structure, this study uses a rectangular plate clamped at all four edges, with dimensions $545\,\text{mm} \times 400\,\text{mm} \times 3\,\text{mm}$. The material constituing the plate is assumed to follow the linear, elastic, isotropic behavior. The typical properties of aluminum were used, with density $2700\,\text{kg}\,\text{m}^{-3}$, Young modulus 69 GPa, Poisson's ration 0.33. The sensors and actuators used for vibration control are square piezoelectric patches with dimensions $25\,\text{mm} \times 25\,\text{mm} \times 0.5\,\text{mm}$, bonded on one of the free surfaces of the plate. The properties of PIC-151 were used, whose values were taken from Physik Instrumente, with missing coefficients calculated as in Chevallier, Ghorbel and Benjeddou (2008).

The patches can take places at predefined grid of 16 per 12 vacancies, as the example in Fig. 2. Four patches fixed at the centre, on positions 88, 89, 104 and 105, are used as actuators. Then 16 sensor patches may be arbitrarily placed on the remaining positions of the grid. The problem consists of finding the positioning which best suits active vibration control when using spatial filters with direct velocity feedback (DVF). Note that, because every piezoelectric patch is installed on the same side of the plate, this problem does not allow perfect collocalization of pairs of sensor and actuator. In order to access the performance, a punctual force normal to the plate will be applied at the point $P = (235, 158)\text{mm}$ and the displacement at this point will be measured. For comparison purposes, an optimization of the spatial filter gains with fixed sensors were also performed, with placement as given in Fig. 2.

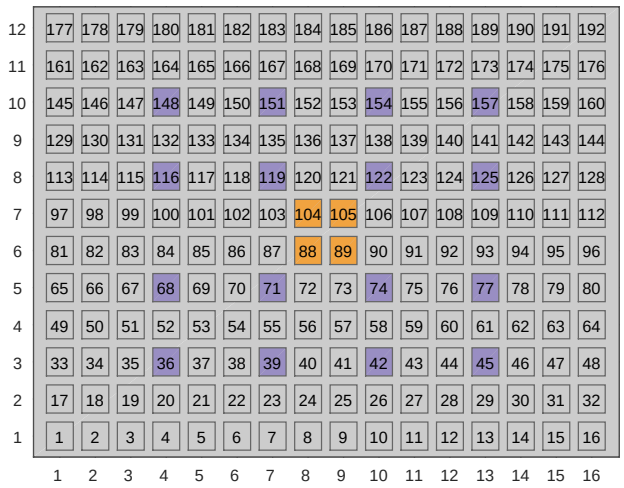

Figure 2: Grid of admissible positions for the piezoelectric patches. In this example, sensors were colored in purple while actuators were colored in orange.

When the sensor placement is specified, it is possible then to construct a finite element model for simulation purposes. In this work, we used the finite element formulation for the sandwich piezoelectric plate as developed in Santos and Trindade (2011). The output is then a system of second-order differential equations of the form

$$\begin{bmatrix} \boldsymbol{M} & \mathbf{0} & \mathbf{0} \\ \mathbf{0} & \mathbf{0} & \mathbf{0} \\ \mathbf{0} & \mathbf{0} & \mathbf{0} \end{bmatrix} \begin{bmatrix} \ddot{\boldsymbol{u}} \\ \ddot{\boldsymbol{q}}_s \\ \ddot{\boldsymbol{q}}_a \end{bmatrix} + \begin{bmatrix} \boldsymbol{K}_u & -\boldsymbol{K}_{uqs} & -\boldsymbol{K}_{uqa} \\ -\boldsymbol{K}_{uqs}^T & -\boldsymbol{K}_{qs} & 0 \\ -\boldsymbol{K}_{uqa}^T & 0 & -\boldsymbol{K}_{qa} \end{bmatrix} \begin{bmatrix} \boldsymbol{u} \\ \boldsymbol{q}_s \\ \boldsymbol{q}_a \end{bmatrix} = \begin{bmatrix} \boldsymbol{f}(t) \\ \boldsymbol{V}_s(t) \\ V_a(t) \end{bmatrix}, \tag{1}$$

where, $\boldsymbol{M}$ is the inertia matrix; $\boldsymbol{K}_u$ is the mechanical stiffness matrix; $\boldsymbol{K}_{qs}$ and $\boldsymbol{K}_{qa}$ are dielectric stiffness matrices of sensors and actuators; $\boldsymbol{K}_{uqs}$ and $\boldsymbol{K}_{uqa}$ are piezoelectric stiffness matrices; $\boldsymbol{u}$ is a vector containing mechanical degrees of freedom; $\boldsymbol{q}_s$ and $\boldsymbol{q}_a$ are vectors containing electrical charges degrees of freedom; $\boldsymbol{f}(t)$ is an external force being applied on point P; $\boldsymbol{V}_s(t)$ is a vector of electrical voltages induced in the sensors; $V_a(t)$ is the prescribed voltage applied to the actuating patches.

The finite element model typically contains a large number of degrees of freedom, so it is convenient to perform a model reduction so that future computations will be less costly. The system is then transformed to modal coordinates and truncated to the first 80 modes of vibration, yielding a model with natural frequencies present in the range from 100 Hz to 4000 Hz.

When designing a control system in the frequency domain, one has to specify the frequency range over which the control system must accomplish its task. So denote such frequency range by the interval $[f_{min}, f_{max}]$, where f_{min} and f_{max} are the lower and upper extremes, respectively. Then the control system is designed such that only the modes in the range $[f_{min}, f_{max}]$ are guaranteed to be stable. In the present study, f_{min} is always 100 Hz, while f_{max} can take any value in the range [500, 4000]Hz, because during multiobjective optimization f_{max} is considered to be one of the optimization variables. The equations of the model in modal space with a truncated number of modes are of the form:

$$\ddot{\boldsymbol{\eta}} + \boldsymbol{\Lambda}\dot{\boldsymbol{\eta}} + \boldsymbol{\Omega}^2\boldsymbol{\eta} = \boldsymbol{\Phi}^T\boldsymbol{f}(t) + \boldsymbol{\Phi}^T\boldsymbol{K}_{uva}V_a \tag{2}$$

$$\boldsymbol{V}_s = -\boldsymbol{K}_{uqs}^T\boldsymbol{\Phi}\boldsymbol{\eta}, \tag{3}$$

where $\boldsymbol{\Lambda}$ is a matrix of modal damping; $\boldsymbol{\Omega}^2$ is a diagonal matrix whose elements are the square of the natural frequencies; $\boldsymbol{\Phi}$ is a matrix whose columns are the eigenvectors associated to the 50 first vibration modes, normalized such that $\boldsymbol{\Phi}^T\boldsymbol{M}\boldsymbol{\Phi} = \boldsymbol{I}$, where $\boldsymbol{I}$ is the identity matrix. The vector $\boldsymbol{\eta}$ is obtained from the transformation $\boldsymbol{u} = \boldsymbol{\Phi}\boldsymbol{\eta}$. Let $\boldsymbol{z} = [\,\boldsymbol{\eta} \;\; \dot{\boldsymbol{\eta}}\,]^T$ the state vector of the system. Then it is possible to represent the system in state-space form:

$$\dot{\boldsymbol{z}} = \boldsymbol{A}\boldsymbol{z} + \boldsymbol{B}_f f(t) + \boldsymbol{B}_a V_a(t) \tag{4}$$

$$u_p = \begin{bmatrix} \boldsymbol{C}_u\boldsymbol{\Phi} & \mathbf{0} \end{bmatrix}\boldsymbol{z} = \boldsymbol{C}_p\boldsymbol{z} \tag{5}$$

$$v_p = \dot{u}_p = \begin{bmatrix} \mathbf{0} & \boldsymbol{C}_u\boldsymbol{\Phi} \end{bmatrix}\boldsymbol{z} = \boldsymbol{C}_v\boldsymbol{z} \tag{6}$$

$$\boldsymbol{V}_s = \begin{bmatrix} \boldsymbol{K}_{uqs}^T\boldsymbol{\Phi} & \mathbf{0} \end{bmatrix}\boldsymbol{z} = \boldsymbol{C}_{vs}\boldsymbol{z} \tag{7}$$

$$\dot{\boldsymbol{V}}_s = \begin{bmatrix} \mathbf{0} & \boldsymbol{K}_{uqs}^T\boldsymbol{\Phi} \end{bmatrix}\boldsymbol{z} = \boldsymbol{C}_{dvs}\boldsymbol{z}, \tag{8}$$

where the index P in u_P indicates that the measurement of displacement is taken at point P.

The open-loop receptance at point P may be found by ignoring the active forces f_a the piezoelectric actuators exert on the plate, followed by the Laplace transform of (4), yielding

$$\boldsymbol{z}s = \boldsymbol{A}\boldsymbol{z} + \boldsymbol{B}_f f(t). \tag{9}$$

Isolate $\boldsymbol{z}$ in (9) and combine with (5) to arrive at

$$u_p(s) = \boldsymbol{C}_u \boldsymbol{\Phi}(\boldsymbol{I}s - \boldsymbol{A})^{-1}\boldsymbol{B}_f f(s) = H_{uf}(s) f(s). \tag{10}$$

Equation (10) may be used to find the open-loop receptance $H_{uf}(\omega)$ of the plate at point P by making $s = i\omega$.

The output of the spatial filter is, according to the convention used in Preumont et al. (2003),

$$y(t) = \boldsymbol{\alpha}^T \boldsymbol{V}_s. \tag{11}$$

When using the derivative of the sampled signal, a low-pass filter is usually included in the feedback loop in order to avoid extremely large amplitudes in higher portion of the frequency bandwidth. Assume a general state-space representation of a single input, single output (SISO) filter as

$$\dot{\boldsymbol{q}} = \boldsymbol{G}\boldsymbol{q} + \boldsymbol{H}y \tag{12}$$

$$w = \boldsymbol{J}\boldsymbol{q} + \boldsymbol{L}y, \tag{13}$$

where $\boldsymbol{G}$, $\boldsymbol{H}$, $\boldsymbol{J}$ and $\boldsymbol{L}$ are the matrices of the filter $F(s)$ in state-space representation, $\boldsymbol{q}$ is a vector containing the internal states of the filter $T(s)$, y is the signal from the spatial filter and w is the filtered output. In this study, a 6th order Butterworth filter was used, with cutoff frequency f_{cut} calculated during the optimization routine.

The DVF control law has the form

$$V_a(t) = -K\dot{w} = -K(\boldsymbol{J}\dot{\boldsymbol{q}} + \boldsymbol{L}\dot{y}) \tag{14}$$

After combining Eqs. (4), (5), (8), (11), (12), (13) and (14), the state-space formulation of the closed-loop system can be found to be

$$\begin{bmatrix} \dot{\boldsymbol{z}} \\ \dot{\boldsymbol{q}} \end{bmatrix} = \begin{bmatrix} \boldsymbol{A} - K\boldsymbol{B}_a\boldsymbol{J}\boldsymbol{H}\boldsymbol{\alpha}^T\boldsymbol{C}_{vs} - K\boldsymbol{B}_a\boldsymbol{L}\boldsymbol{\alpha}^T\boldsymbol{C}_{dvs} & -K\boldsymbol{B}_a\boldsymbol{J}\boldsymbol{G} \\ \boldsymbol{H}\boldsymbol{\alpha}^T\boldsymbol{C}_{vs} & \boldsymbol{G} \end{bmatrix} \begin{bmatrix} \boldsymbol{z} \\ \boldsymbol{q} \end{bmatrix} + \begin{bmatrix} \boldsymbol{B}_f \\ \boldsymbol{0} \end{bmatrix} f \tag{15}$$

$$u_p = \begin{bmatrix} \boldsymbol{C}_p & \boldsymbol{0} \end{bmatrix} \begin{bmatrix} \boldsymbol{z} \\ \boldsymbol{q} \end{bmatrix} \tag{16}$$

$$V_a = -\begin{bmatrix} K\boldsymbol{J}\boldsymbol{H}\boldsymbol{\alpha}^T\boldsymbol{C}_{vs} + K\boldsymbol{L}\boldsymbol{\alpha}^T\boldsymbol{C}_{dvs} & K\boldsymbol{J}\boldsymbol{G} \end{bmatrix} \begin{bmatrix} \boldsymbol{z} \\ \boldsymbol{q} \end{bmatrix}. \tag{17}$$

In short,

$$\dot{\boldsymbol{z}}_e = \boldsymbol{A}_{cl}\boldsymbol{z}_e + \boldsymbol{B}_{cl} f \tag{18}$$

$$u_p = \boldsymbol{C}_{pcl}\boldsymbol{z}_e \tag{19}$$

$$V_a = -\boldsymbol{V}_{acl}\boldsymbol{z}_e, \tag{20}$$

where $\boldsymbol{z}_e = [\boldsymbol{z}\ \boldsymbol{q}]^T$.

Apply the Laplace Transform to Eq. (18) and isolate $\boldsymbol{z}$, to arrive at

$$\boldsymbol{z}_e(s) = (\boldsymbol{I}s - \boldsymbol{A}_{cl})^{-1}\boldsymbol{B}_f f(s). \tag{21}$$

The closed-loop displacement measured at point P and the control effort can, in turn, be determined from Eqs. (19), (20), and (21), yielding

$$u_p(s) = \boldsymbol{C}_{pcl}(\boldsymbol{I}s - \boldsymbol{A}_{cl})^{-1}\boldsymbol{B}_f f(s) = H_{pf}(s) f(s) \tag{22}$$

$$V_a(s) = -V_{acl}(\boldsymbol{I}s - \boldsymbol{A}_{cl})^{-1}\boldsymbol{B}_f f(s) = H_{vaf}(s) f(s). \tag{23}$$

Thus the FRF with harmonic force input $f(\omega)$ and displacement output $u_p(\omega)$, henceforth denominated H_{pf}, may be found by evaluating Eq. (22) after applying the transformation $s = i\omega$ over the desired frequency range. Likewise, the FRF with harmonic force input $f(\omega)$ and control effort output $V_a(\omega)$, henceforth denominated H_{vaf}, may be found after following the same procedure with Eq. (23).

It would be desirable to keep at minimum the maximum amplitude of both $u_p(\omega)$ and $V_a(\omega)$, but these quantities are inversely related, that is, one increases whenever the other decreases. The designer consequently has to choose a

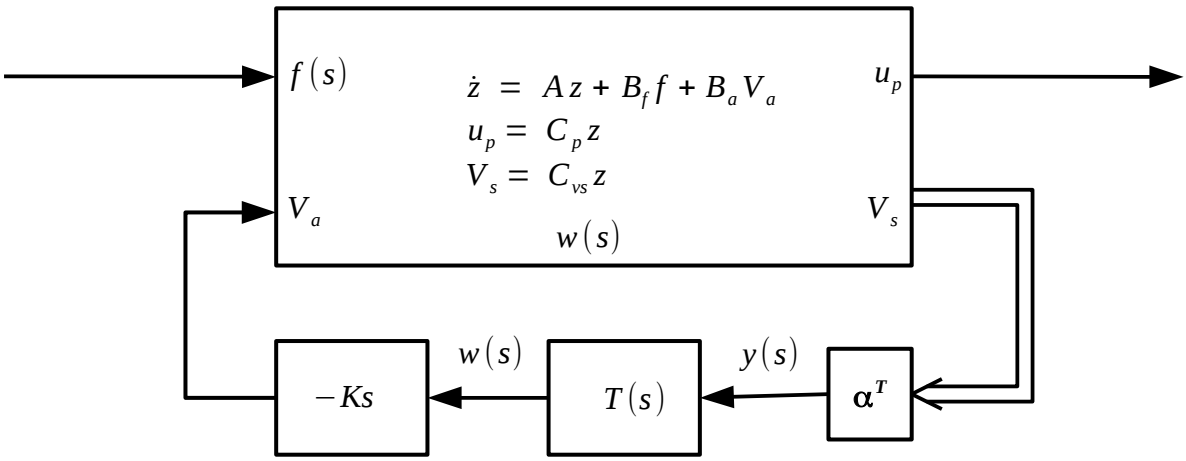

Figure 3: Representation of the dynamic model of the vibrating plate and its control system in block diagram.

compromise between performance and control effort. Besides, the compromise also changes whenever we consider a larger or a shorter frequency band of operation. In order to quantify vibration attenuation in each mode, the following metric J_Q was stablished: suppose that the first m modes are inside the frequency band $[f_{min}, f_{max}]$ where the control system must perform. Then define

$$J_Q = \sum_{j=1}^{m} W_j \frac{|H_{pf}(\omega_{n,j})|}{|H_{uf}(\omega_{n,j})|}, \tag{24}$$

where W is a m-vector of weighting coefficients and $\omega_{n,j}$ is the natural frequency of the j-th mode in the open loop model. Note that H_{pf} is the closed-loop receptance at point P, as defined according to (22), while H_{uf} is the open-loop receptance at point P, as defined according to (10). For this study, the following configuration for W was chosen

$$\begin{aligned} &W_j = 1 \quad \text{if } j \in \{1,4,8\} \\ &W_j = 0.1 \quad \text{if } j \notin \{1,4,8\} \text{ and } j \leq 10 \\ &W_j = 0.01 \quad \text{otherwise} \end{aligned}$$

Thus J_Q is a weighted sum of the values $H_{pf}(\omega)$ normalized by $H_{uf}(\omega)$ takes at the open-loop natural frequencies. This study will use J_Q as a measure of performance, where lower values of J_Q mean better vibration attenuation. The penalization of high control efforts will be accomplished by stablishing an upper limit of control voltage, as detailed in the next section.

The optimization problem is then stated as follows: find the Pareto front of the pair of functions $(J_Q(\boldsymbol{x}, \boldsymbol{\alpha}, f_cut, f_{max}), -f_{max})$, where $\boldsymbol{x}$ is a vector of length 16 containing integers randomly sampled without repetition from the set $\{1,2,\ldots,192\} \setminus \{88,89,104,105\}$; $\boldsymbol{\alpha}$ is a unitary vector of length 16 where the j-th element represents the coefficient of the j-th input of the spatial filter; f_{max} is the upper end of the frequency range used to access the performance of the individue.

Design of the optimal feedback control gain K

The previous section defined a way to measure the closed-loop performance, but did not specify a way to find α nor K. This section describes the procedure for finding K, while the vector of gains α will be found via Genetic Algorithm.

The open-loop system, that is, with null feedback gain $K = 0$, will have the structure's natural damping and the control effort will be null, as no control feedback is being used. Thus, when $K = 0$ the system is always feasible. One can then increase K until either the minimum modal damping or the maximum control effort (or both) is violated. At this point, the search halts and the greatest feasible gain is taken as the optimal feedback gain for the DVF control law. The procedure used here is then as follows: if the closed-loop system has acceptable damping and control effort not above the stipulated limit, then make the performance index J defined to be equal to J_Q, as defined in Eq. (24). Otherwise, it is defined to be an extremely high value, which in this study was set to 1×10^6. Then,

$$J = \begin{cases} J_Q & \text{if } \xi_j > 0.25\% \quad \text{and} \quad \max\limits_{100\,\text{Hz} \leq r \leq f_{max}} \dfrac{V_a}{F}(2\pi r) \leq 200\text{V/N} \\ 1 \times 10^6 & \text{otherwise} \end{cases} \tag{25}$$

Note that a linear search is considerably costly, specially if K is to be computed within a low tolerance, since the number

of iterations grows at order $O(10^n)$, where n is the number of significant digits. In this work, dichotomy search Rao (2009) was used as the computational complexity grows linearly with the number of significant digits, at order $O(n)$.

Formulation of Genetic Algorithm

When performing the multiobjective optimization with fixed sensors, all optimization variables are real, with 16 variables of type double in the range $[-1,1]$ representing the gains of the spatial filter, one variable of type double in the range $[0,1]$ used to represent the ratio $r_c = f_{cut}/f_{max}$ between the cutoff frequency of the low pass filter and f_{max}. The last variable is of the type double in the range $[500,4000]$Hz and it represents f_{max}. The crossover is implemented via arithmetic mean, with normalization of the vector consisting of the 16 gains via Euclidean norm. Such strategy was used in order to avoid having different individues representing the same modal sensor. The mutation was implemented using Gaussian mutation with Scale and Shrink parameters both set to 1. After performing the mutation, the vector of gains is normalized as well, again to avoid having multiple individues representing the same modal sensor. The default options were kept for the remaining Genetic Algorithm operations from MATLAB's Global Optimization Toolbox.

When performing the multiobjective optimization including sensor placement, the optimization becomes of the mixed integer type. In order to comply with the requirements of this study's model, it was necessary to supply custom routines for the initial population, for the crossover and for the mutation operations to be compatible with the way the information is organized in the cromossome, which is of the format

$$[x_1, x_2, \ldots, x_{16}, \alpha_1, \alpha_2, \ldots, \alpha_{16}, r_c, f_{max}], \tag{26}$$

where $x_j \in \{1,2,\ldots,192\}$ denotes the position of the j-th sensor, $\alpha_j \in [-1,1]$ denotes the gain of the j-th sensor in the modal filter construction, r_c denotes the ratio f_{cut}/f_{max} and f_{max} denotes the upper bound of the frequency band where the control system is designed.

Crossover. The crossover operation is performed on each part of the cromossome separately. Let

$$\begin{aligned}
[x_1, x_2, \ldots, x_{16}, \alpha_1, \alpha_2, \ldots, \alpha_{16}, f_{cut,1}, f_{max,1}] &\quad \text{denote the first parent,} \\
[y_1, y_2, \ldots, y_{16}, \beta_1, \beta_2, \ldots, \beta_{16}, f_{cut,2}, f_{max,2}] &\quad \text{denote the second parent and} \\
[z_1, z_2, \ldots, z_{16}, \gamma_1, \gamma_2, \ldots, \gamma_{16}, f_{cut}, f_{max}] &\quad \text{denote their child.}
\end{aligned}$$

The detailed steps are as follows:

1. From the first parent, associate the position of each sensor with its gain by making pairs of the form $P_j = (x_j, \alpha_j)$. Do the same for the second parent. Make a collection C of all pairs that were created in step 1.
2. There may be pairs P_j, P_k in C at the same position which came from different parents. In such case, update their gain values as $\alpha'_j \leftarrow \text{mean}(\alpha_j, \beta_k)$ and $\beta'_k \leftarrow \text{mean}(\alpha_j, \beta_k)$.
3. Randomly sample 16 pairs from C. Each time a pair (z_j, γ_j) is sampled, there may be another pair C with same position z_j. Remove it from C.
4. From the 16 pairs sampled in step 4, $f_{cut} \leftarrow \text{mean}(f_{cut,1}, f_{cut,2})$ and $f_{max} \leftarrow \text{mean}(f_{max,1}, f_{max,2})$, create the cromossome for a new individue, that will represent the child of the two parents.

The way the crossover is implemented guarantees that there will be no patch superposition in the child. Besides, the sensor gains are moved around with their corresponding positions to keep the child sensors consistent with its parent's ones.

Mutation. The mutation operation is performed separately on each part of the cromossome as well, but in this case there is no need to create pairs as in the crossover operation. So, assuming an individue of the form

$$[x_1, x_2, \ldots, x_{16}, \alpha_1, \alpha_2, \ldots, \alpha_{16}, f_{cut}, f_{max}], \tag{27}$$

take the following steps:

1. for each $j \in \{1,2,\ldots,16\}$, randomly sample a position $x'_j \in \{1,2,\ldots,192\} \setminus \{x_1, x_2, \ldots, x_{16}\}$ and update $x_j \leftarrow x'_j$ with probability $p = 0.01$;
2. for the gains $[\alpha_1, \alpha_2, \ldots, \alpha_{16}]$, perform a Gaussian mutation with Scale and Shrink parameters equal to 1 and normalize the vector of gains $[\alpha_1, \alpha_2, \ldots, \alpha_{16}]$.
3. for f_{cut} and f_{max}, perform a Gaussian mutation with Scale and Shrink equal to 1 and later enforce that both are inside their respective bounds by truncating, if necessary.

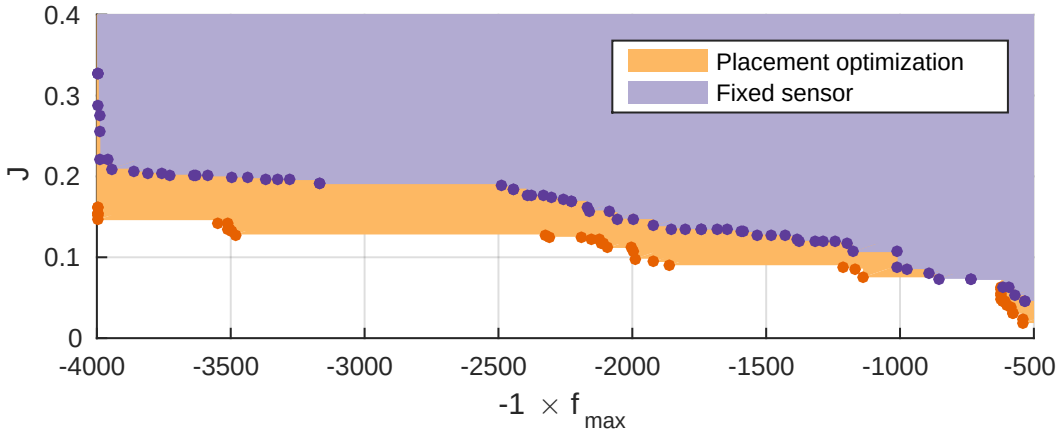

Figure 4: Pareto fronts for the cases with simultaneous optimization of sensor gains and placement (purple) and optimization of sensor gains with fixed placement (orange). The purple region was plotted over the orange.

RESULTS

Both the multiobjective optimization with fixed sensors and the one optimizing sensor placement were carried on a population of 196 individues over 200 generations. The resulting Pareto fronts and their dominance regions can be ascertained from Fig. 4. As expected, the optimization with sensor placement dominates the optimization with fixed sensors, at least as far as the metric J_Q is concerned. In order to access more accurately the performance of both systems, the frequency response of both strategies of optimization are compared in three different values for f_{max}: 850 Hz (12 modes present in the frequency band), 1800 Hz (28 modes present in the frequency band), 3200 Hz (55 modes present in the frequency band). Those FRFs are plotted in Fig. 5, 6 and 7. The dotted lines indicate the open-loop (OL) receptances at point P, while the solid lines indicate the closed-loop (CL) response. An examination of Fig. 6 shows that it is possible to attenuate the vibration associated to the target modes 1, 4 and 8 with the rectangular grid of sensors, but sensor placement optimization improves performance, as expected from the Pareto fronts in Fig. 4. In this case, fixed sensors attenuates the modes 1, 4 and 8 by -18, -19 and -19 dB while sensor placement optimization gives -24, -18 and -23 dB of attenuation. The difference is more evident as the upper bound of the design frequency band rises to 3200 Hz. For the system optimized with fixed sensors, the attenuations for the modes 1, 4 and 8 are -13, 4, and -12 dB, while the system optimized with sensor placement attenuates by -22, -19 and -17 dB, respectively. Its is also noteworthy that the 5th mode, at 403 Hz was attenuated by 10 dB even though it was not explicitly required to be attenuated. The stability of the system designed for $f_{max} = 3200$ Hz was also checked on the model with all modes of vibration up to 4000 Hz. Thanks to the low-pass filter, the potential instabilities caused by spillover were avoided, as the effect of the spatial filter became negligible in higher frequencies, and the closed-loop system remained stable.

CONCLUSIONS

The results obtained from LSQ as traditionally proposed in the literature depend too much on the initial target function to be approximated, delivering a suboptimal control design. By performing a closed loop optimization of the system using GA, it was possible to find a feedback matrix which made better use of the control effort, leading to more effective control of the modes 1, 4 and 8, even including some extra attenuation at other modes which were not required to be controlled.

It was observed that by including sensor placement into the optimization procedure, the frequency bandwidth of operation can be increased with less performance loss than the case with fixed sensors.However, sensor placement optimization alone will not always guarantee a visibly better outcome. For example, if the optimization were carried on a fixed f_{max} between 500 Hz and 1000 Hz, there would be no significant benefit. It is thus recommendable to perform a multiobjective optimization on a wide range of frequencies so that the one knows the values of f_{max} for which sensor placement gives an advantage over fixed sensors.

ACKNOWLEDGMENTS

Support of MCT/CNPq/FAPEMIG National Institute of Science and Technology on Smart Structures in Engineering, 574001/2008-5, and National Council for Scientific and Technological Development (CNPq), 309193/2014-1 and 142256/2015-3, are acknowledged

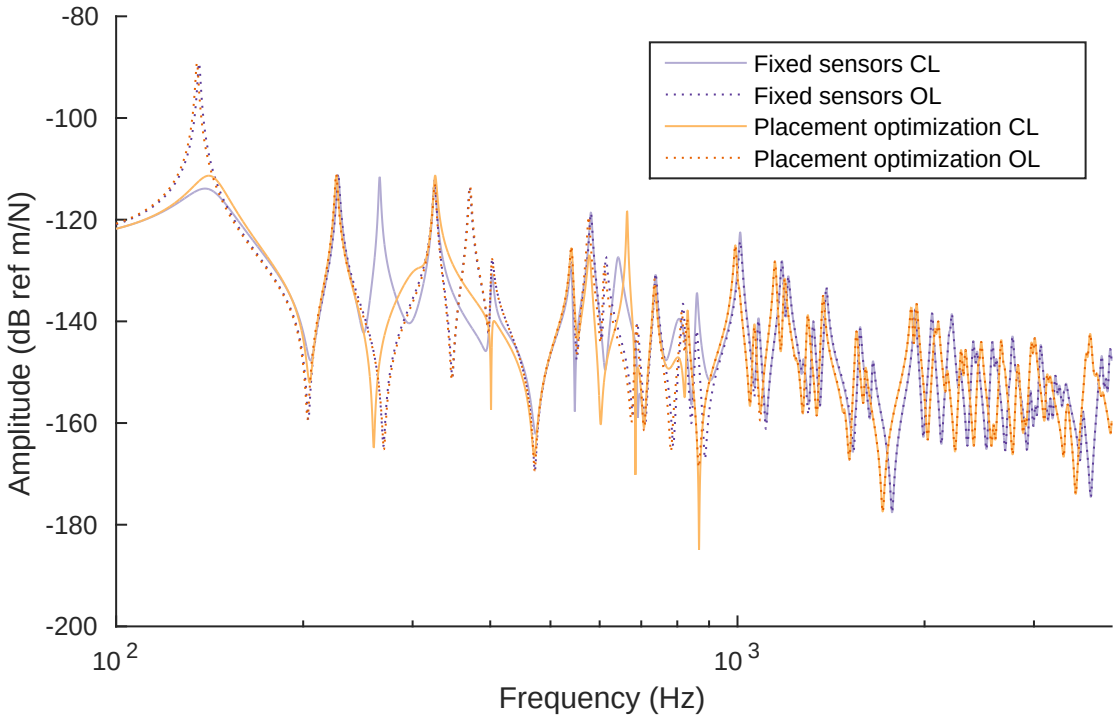

Figure 5: The FRF of the closed loop optimal systems for $f_{max} = 850\,\text{Hz}$.

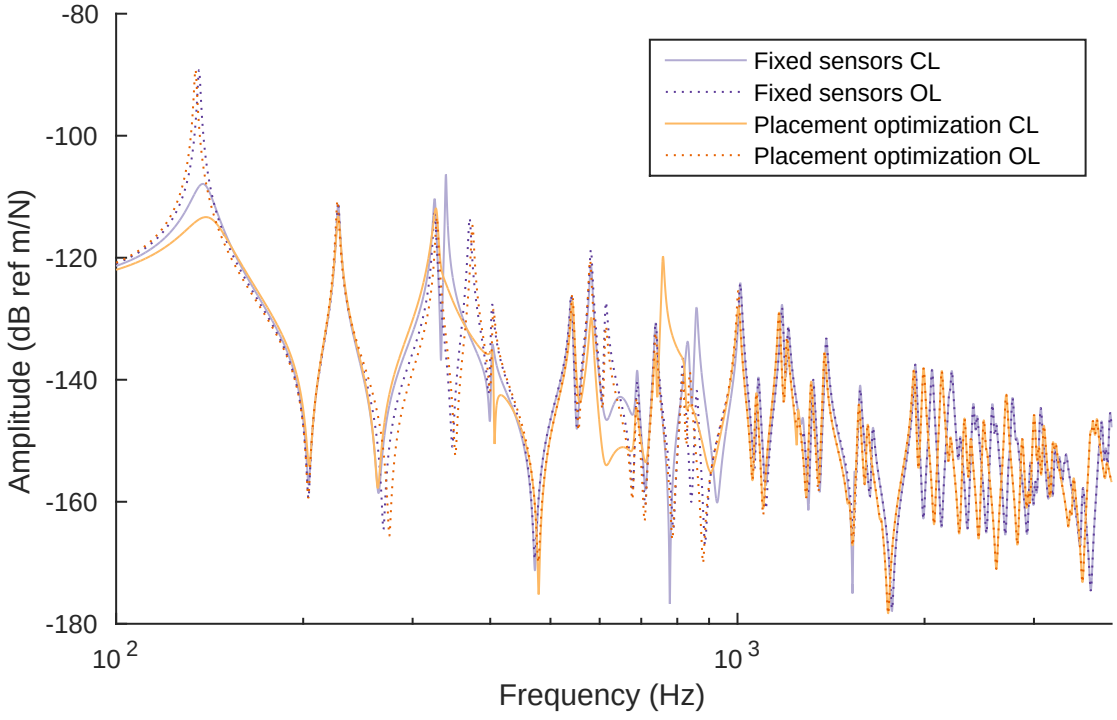

Figure 6: The FRF of the closed loop optimal systems for $f_{max} = 1800\,\text{Hz}$.

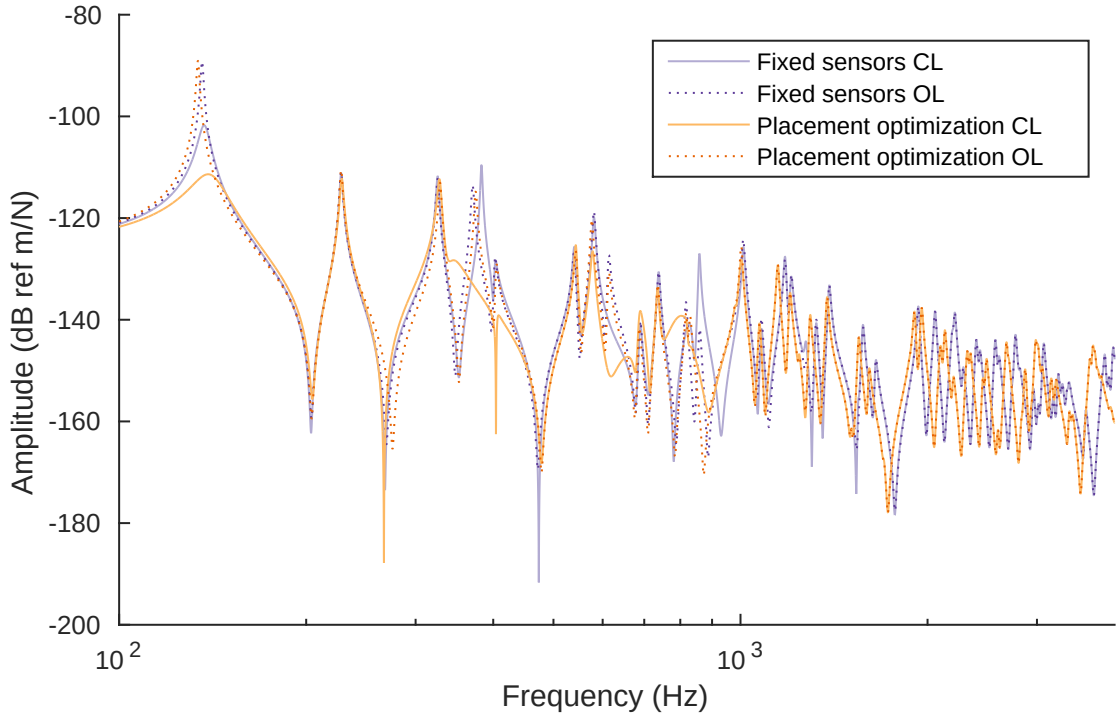

Figure 7: The FRF of the closed loop optimal systems for $f_{max} = 3200\,\text{Hz}$.

REFERENCES

Biglar, M., Gromada, M., Stachowicz, F. and Trzepieciński, T. (2015), "Optimal configuration of piezoelectric sensors and actuators for active vibration control of a plate using a genetic algorithm", Acta Mechanica, vol. 226, no. 10, pp. 3451–3452.

Chevallier, G., Ghorbel, S. and Benjeddou, A. (2008), "A benchmark for free vibration and effective coupling of thick piezoelectric smart structures", Smart Materials and Structures, vol. 17, no. 6.

Cinquemani, S., Ferrari, D. and Bayati, I. (2015), "Reduction of spillover effects on independent modal space control through optimal placement of sensors and actuators", Smart Materials and Structures, vol. 24, no. 8.

Cruz Neto, H.J. (2018), Otimização de posicionamento de sensores e atuadores para o controle com realimentação de saída utilizando critério de desempenho quadrático, Master's thesis, São Carlos School of Engineering, University of São Paulo, available at: <http://www.teses.usp.br/teses/disponiveis/18/18149/tde-25052018-174813/en.php>.

Cruz Neto, H.J. and Trindade, M.A. (2017), "Optimal placement of sensors for the output feedback control of structures using quadratic performance criterion", in: Proceedings of the 24th Brazilian Congress of Mechanical Engineering, Curitiba, Brazil.

Gonçalves, J.F., de Leon, D.M. and Perondi, E.A. (2017), "Topology optimization of embedded piezoelectric actuators considering control spillover effects", Journal of Sound and Vibration, vol. 388, no. 3, pp. 20–41.

Gupta, V., Sharma, M. and Takur, N. (2010), "Optimization criteria for optimal placement of piezoelectric sensors and actuators on a smart structure: a technical review", Journal of Intelligen Material Systems and Structures, vol. 21, no. 12, pp. 1227–1243.

Han, J.H. and Lee, I. (1999), "Optimal placement of piezoelectric sensors and actuators for vibration control of a composite plate using genetic algorithms", Smart Materials and Structures, vol. 8, no. 2, pp. 257–267.

Horiy, F.M., Shigueoka, A.H. and Trindade, M.A. (2017), "Analysis of piezoelectric sensor networks for spatial modal filters and active vibration control", in: Proceedings of the 24th Brazilian Congress of Mechanical Engineering, Curitiba, Brazil.

Hsu, C.Y., Lin, C.C. and Gaul, L. (1998), "Vibration and sound radiation controls of beams using layered modal sensors and actuators", Smart Materials and Structures, vol. 7, no. 4, pp. 446–455.

Khushnood, M.A., Xiaogang, W. and Naigang, C. (2018), "A criterion for optimal sensor placement for minimizing spillover effects on optimal controllers", Journal of Vibration and Control, vol. 24, no. 8, pp. 1469–1487.

Leo, D.J. (2007), Engineering Analysis of Smart Materials Systems, John Wiley & Sons.

Meirovitch, L. (1990), Dynamics and control of structures, Willey.

Meirovitch, L. and Baruh, H. (1982), "Control of Self-Adjoint Distributed-Parameter Systems", Journal of Guidance, Control, and Dynamics, vol. 5, no. 1, pp. 60–66.

Meirovitch, L. and Öz, H. (1980), "Modal-Space control of distributed gyroscopic system", Journal of Guidance, Control and Dynamics, vol. 3, no. 2, pp. 140–150.

Pagani, Jr, C.C. and Trindade, M.A. (2009), "Optimization of modal filters based on arrays of piezoelectric sensors", Smart Materials and Structures, vol. 18, no. 9, pp. 1–12.

Physik Instrumente (), "Material data - specific parameters of the standard materials", Available at https://www.physikinstrumente.com/en/technology/piezo-technology/piezoelectric-materials/, time of access: 13 Sept. 2018.

Preumont, A., François, A., de Man, P. and Piefort, V. (2003), "Spatial filters in structural control", Journal of Sound and Vibration, vol. 265, no. 1, pp. 61–79.

Rao, S.S. (2009), Engineering optimization: theory and practice, Wiley, 4th ed.

Sadri, A.M., Wright, J.R. and Wynne, R.J. (1999), "Modelling and optimal placement of piezoelectric actuators in isotropic plates using genetic algorithms", Smart Materials and Structures, vol. 4, no. 8, pp. 490–498.

Santos, H.F.L. and Trindade, M.A. (2011), "Structural vibration control using extension and shear active-passive piezoelectric networks including sensitivity to electrical uncertainties", Journal of the Brazilian Society of Mechanical Sciences and Engineering, vol. 33, no. 3.

Xue, K., Igarashi, A. and Kachi, T. (2018), "Optimal sensor placement for active control of floor vibration considering spillover effect associated with modal filtering", Engineering Structures, vol. 165, pp. 198–209.

RESPONSIBILITY NOTICE

The authors are the only responsible for the printed material included in this paper.